Fibers and Polymers 2013, Vol.14, No.8, 1332-1338 DOI 10.1007/s12221-013-1332-8

Structures and Physical Properties of Graphene/PVDF Nanocomposite Films Prepared by Solution-mixing and Melt-compression

Jin Woo Jang, Byung Gil Min, Jeong Hyun Yeum[1], and Young Gyu Jeong*

Department of Materials Design Engineering, Kumoh National Institute of Technology, Gumi 730-701, Korea
[1]Department of Advanced Organic Materials Science and Engineering, Kyungpook National University, Daegu 702-701, Korea

(Received January 31, 2013; Accepted February 21, 2013)

Abstract: We have manufactured poly(vinylidene fluoride) (PVDF)-based nanocomposite films with different graphene contents of 0.1~10.0 wt% by ultrasonicated solution-mixing and melt-compression. As a reinforcing nanofiller, graphene sheets are prepared by rapid thermal expansion of graphite oxide, which are from the oxidation of natural graphite flakes. Graphene sheets are characterized to be well exfoliated and dispersed in the nanocomposite films. X-ray diffraction data confirm that the α-phase crystals of PVDF are dominantly developed in the nanocomposite films during the melt-crystallization. DSC cooling thermograms show that the graphene sheets serve as nucleating agents for the PVDF α-form crystals. Thermal stability of the nanocomposite films under oxygen gas atmosphere is noticeably improved, specifically for the nanocomposite with 1.0 wt% graphene. Electrical volume resistivity of the nanocomposite films is substantially decreased from ~10^{14} to ~10^{6} W cm, especially at a critical graphene content between 1.0 and 3.0 wt%. In addition, mechanical storage modulus is highly improved with increasing the graphene content in the nanocomposite films. The increment of the storage modulus for the nanocomposite film at 30 ^{o}C with increasing the graphene content is analyzed by adopting the theoretical model proposed by Halpin and Tsai.

Keywords: Poly(vinylidene fluoride), Graphene, Nanocomposite, Mechanical property, Electrical property

Introduction

Poly(vinylidene fluoride) (PVDF) is highly non-reactive thermoplastic material in the fluoropolymer family that exhibits good resistance to high temperatures, UV irradiation and aggressive chemicals [1,2]. Since PVDF has a low density of ~1.78 and low cost compared with the other fluoropolymers, it has been used as piping products, sheets, tubing, films, filaments, plates and a insulator for premium wire. It can be injected, molded or welded and is commonly used in the chemical, semiconductor, medical and defense industries, as well as in lithium ion batteries. On the other hand, for the advanced applications requiring electrostatic dissipation and electromagnetic interference, high electrical resistivity of PVDF should be much decreased.

Polymer nanocomposites (PNC) are a class of composites having nano-scale reinforcing fillers dispersed in the polymer matrix, unlike the conventional polymer composites [3-5]. The nano-scale fillers can be of different shape (e.g., platelets, fibers, spheroids), but at least one dimension must be in the range of 1 to 100 nm. The transition from micro- to nano-scale fillers lead to change in physical as well as chemical properties of polymer matrix. Two of the major factors in this are the increase in the ratio of the surface area to volume and the size of the filler. The increase in surface area-to-volume ratio, which increases as the fillers get smaller, leads to an increasing interaction of atoms on the surface area of particle with the polymeric matrix and this thus increases the strength, heat resistance, etc. The PNC systems require controlled mixing/compounding, stabilization of the achieved dispersion, orientation of the dispersed phase, and the compounding strategies.

Among nano-scale reinforcing fillers, graphene sheets, structurally monolayer of carbon atoms arranged in 2-dimensional honeycomb lattice [6], have recently generated enormous attention from industry and academia to attain high performance PNC systems, since they have exceptional structural and physical properties such as high surface area-to-volume ratio [7], thermal stability [8], mechanical performance [9] and electrical conductivity [10]. When incorporated approximately, graphene sheets can dramatically enhance the electrical, physical, mechanical properties of PNC systems at extremely low loadings [11]. Though there have been recent reports on PVDF-based nanocomposites including graphene or its derivatives [12-15], systematic investigations on the influences of graphene sheets on structures, thermal transition, and physical properties of graphene/PVDF nanocomposite films are further needed to pursue. In the present study, we have manufactured a series of PVDF-based nanocomposite films including a variety of graphene content of 0.1~10.0 wt% via ultrasonicated solution mixing and melt-compression, and have scrutinized the crystalline structures, morphological features, melting/crystallization transitions, electrical resistivity, and temperature-dependent storage modulus as a function of graphene content in the nanocomposite films.

*Corresponding author: ygjeong@cnu.ac.kr

Experimental

Materials and Sample Preparation

Poly(vinylidene fluoride) (PVDF) powder ($\overline{M}_w$ ~530,000 g/mol, density~1.76 g/cm^3) was supplied from Scientific Polymer Products, lnc. Natural graphite flake with the average particle diameter of ~500 μm was purchased from Sigma-Aldrich, Inc. Nitric acid (HNO_3, 60 %) and sulfuric acid (H_2SO_4, 90 %) were purchased from Junsei Chemical Co., Ltd. Potassium chlorate ($KClO_3$, 99.5 %) was obtained from Kanto Chemical. Co., Ltd. All the chemicals of analytical grade were used without further purification. Exfoliated graphene as a reinforcing nano-scale filler for PVDF was manufactured by the oxidation of the natural graphite using a mixed $HNO_3/H_2SO_4/KClO_3$ solution and the following rapid thermal expansion of the graphite oxide at 1050 °C for 30 sec [16-19].

Graphene/PVDF nanocomposite films with different graphene contents of 0.1~10.0 wt% were prepared by the processes of ultrasonication-assisted solution mixing, precipitation and melt-compression. PVDF of 20 g was dissolved in 200 m*l* DMF and the predetermined amount of exfoliated graphene was then added. The graphene/PVDF/DMF solutions were mixed mechanically for 1 h and sonicated with a prove-type ultrasonicator for 1 h. Each graphene/PVDF/DMF solution was added drop-wisely into a distilled water bath. Graphene/PVDF precipitates were filtered to obtain in a powdery form. The powers were washed with distilled waters by 3 times and then dried in a vacuum oven at 40 °C for 24 h. Graphene/PVDF nanocomposite films of 200 μm thickness were prepared by melting the dried powders in a hot press at 210 °C for 5 min, transferring rapidly into another hot plate at 25 °C, and then maintaining for 1 h. The graphene contents in the nanocomposites were controlled to be 0.0, 0.1, 0.3, 0.5, 0.7, 1.0, 3.0, 5.0, 7.0, and 10.0 wt%. The final nanocomposite films prepared in this study are coded as graphene/PVDF_X, where X denotes the graphene content by wt% in the nanocomposite films.

Characterization

The dispersion state of graphene sheets in the nanocomposite films was characterized by using a scanning electron microscope (SEM, JEOL JSM-6380LV). For obtaining SEM images, the nanocomposite films were cryogenically fractured in a liquid nitrogen bath. The size of graphene sheets was characterized by using transmission electron microscope (TEM, JEOL/JEM-2100).

Crystalline structures of the neat PVDF and its nanocomposite films with different graphene contents were characterized with aid of an X-ray diffractometer (D/MAX-2000/PC, Rigaku Co.) using nickel-filtered Cu-Kα radiation in the range of 2θ=5~35 ° at a scanning rate of 2 °/min. For comparison, X-ray diffraction patterns of natural graphite and exfoliated graphene sheets were also obtained.

Melting and crystallization behavior of the graphene/PVDF nanocomposite films was investigated with a differential scanning calorimeter (Diamond DSC, Perkin Elmer Inc.). All DSC thermograms were obtained under nitrogen gas atmosphere in the temperature range of 0~200 °C at a heating and cooling rate of 10 °C/min.

Thermal stability of the nanocomposite films under the oxygen gas condition was examined by using a thermogravimetric analyzer (SDT Q500, TA Inc.) from 20 to 600 °C at a heating rate of 20 °C/min.

Temperature-dependent storage modulus of the nanocomposite films with dimensions of 40.0×5.0×0.2 mm^3 was measured by using a dynamic mechanical thermal analyzer (TA Q800, TA Inc.) with a frequency of 1 Hz and amplitude of 15 μm in the temperature range of −50~220 °C at a heating rate of 2 °C/min.

Electrical resistivity of the neat PVDF and its nanocomposite films was measured at room temperature by using an electrometer (6517A, Keithley Inc.) with a resistivity test fixture (8009, Keithley Inc.).

Results and Discussion

Structural and Morphological Features

Figure 1(A) shows the X-ray diffraction patterns of natural graphite and exfoliated graphene nanoplatelets. It was characterized that the neat natural graphite is highly ordered crystalline materials by displaying a sharp diffraction peak at 26.3 °, which corresponds to the *d*-spacing of 0.336 nm. On the other hand, there was no any diffraction peak for exfoliated graphene sheets. It means that the natural graphite flakes were totally exfoliated into graphene sheets by the oxidation of the natural graphite and following rapid thermal expansion. The diameter of exfoliated graphene sheets was measured to be 5~10 μm, as can be seen in the TEM image of Figure 1(B).

To confirm the morphological features of graphene sheets

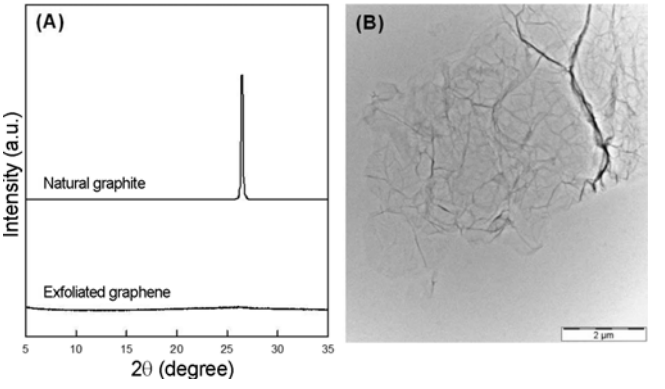

Figure 1. (A) X-ray diffraction patterns of natural graphite flakes and exfoliated graphene sheets and (B) TEM image of graphene sheets obtained by the oxidation, thermal expansion, and ultrasonication.

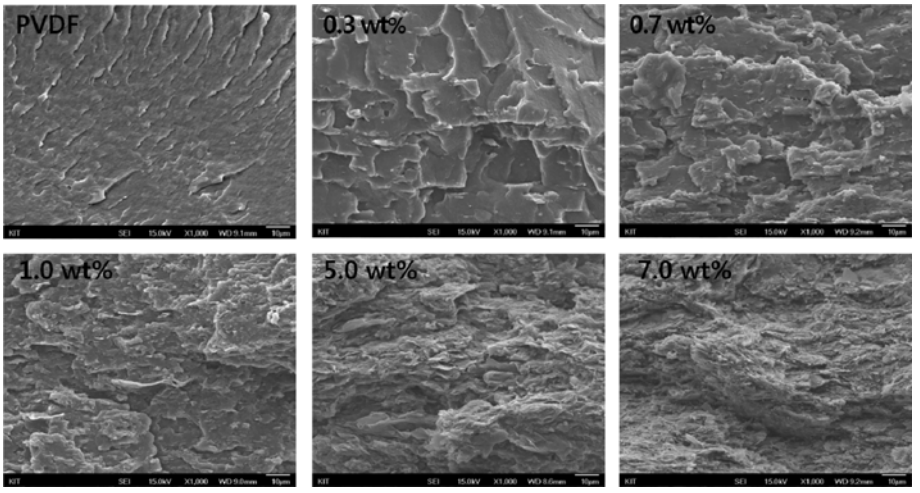

Figure 2. SEM images of fractured surfaces of graphene/PVDF nanocomposite films with different graphene contents.

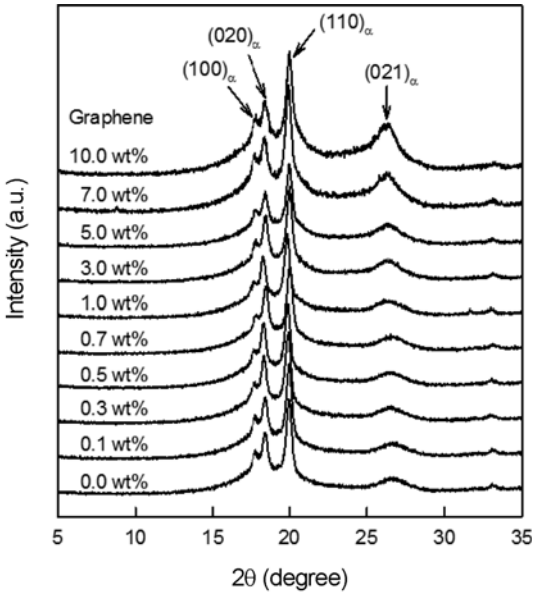

Figure 3. X-ray diffraction patterns of graphene/PVDF nanocomposite films with different graphene contents, which were melt-crystallized at 25 °C.

incorporated in the PVDF matrix, SEM images of the fractured surfaces for the nanocomposite films were examined, as shown in Figure 2. The pristine PVDF film displays a smooth surface (Figure 2(A)). In contrast, the rougher fractured surface was observed for graphene/PVDF nanocomposite films with higher graphene contents (Figure 2(B)-(F)). The nanocomposite films with 0.3 and 0.7 wt% graphene contents exhibit the rough fractured surfaces without aggregates of graphene sheets (Figure 2(B)-(C)). It indicates that the graphene sheets are well dispersed in the PVDF matrix. However, partial aggregates of graphene platelets in the nanocomposites with higher graphene contents above 1.0 wt% were observed. Nonetheless, it was confirmed that the partial aggregates of graphene sheets are not in ordered crystalline state. As can be seen in X-ray diffraction patterns of Figure 3, any diffraction peak associated with the ordered crystalline phase of graphene sheets was not detected, whereas typical diffraction peaks corresponding to PVDF α-form crystals for all the nanocomposite films were detected, irrespective of the graphene content. The strong diffraction peaks at 2θ = 17.6, 18.5, 20.0, and 26.6 ° are assigned to be 100, 020, 100, and 021 reflections of the PVDF α-phase crystals, respectively.

Melting and Crystallization Transitions

DSC heating and cooling thermograms of the neat PVDF and nanocomposite films were shown in Figure 4. In the first heating curves, it was observed that melting endotherms become broader with the increment of the graphene content and their peak temperatures shifted slightly to lower temperatures with broadening (Figure 4(A)). It is speculated that the slightly lower melting temperatures of the nanocomposite films with higher graphene contents in comparison with the neat PVDF are associated with the presence of thin crystals developed during the melt-crystallization at 25 °C and that the broader melting endotherms are caused by the broader distribution in thickness of PVDF α-form crystals developed in the nanocomposite films. In the DSC cooling curves (Figure 4(B)), the melt-crystallization temperatures of the nanocomposite films shifted to higher temperatures with the increment of graphene content up to ~1.0 wt%. It demonstrates that exfoliated graphene sheets serve as effective nucleating agents for PVDF α-form crystals and thus promoted the overall melt-crystallization rates of the nanocomposites. On the other hand, in cases of the nanocomposite films with higher graphene contents above 1.0 wt%, the melt-crystallization peak temperatures were not changed, but the peak areas were slightly decreased with the graphene contents. On the other hand, in the second heating runs (Figure 4(C)), melting

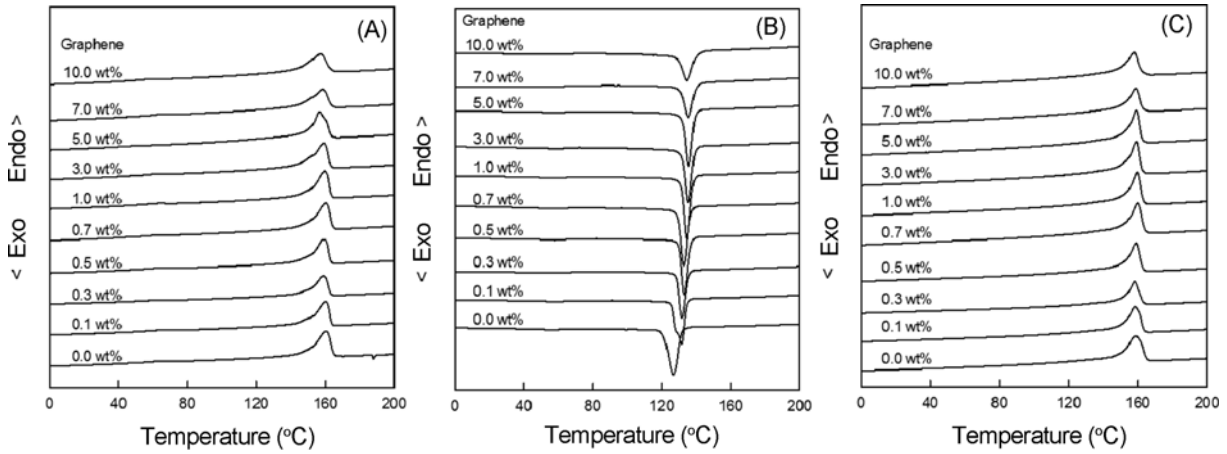

Figure 4. DSC thermograms of graphene/PVDF nanocomposite films with different graphene contents; (A) the first heating curves, (B) the first cooling curves, and (C) the second heating curves.

Table 1. Peak temperatures (T_m and T_c) and enthalpies (ΔH_m and ΔH_c) for melting and crystallization transitions of neat PVDF and graphene/PVDF nanocomposite films with different graphene contents

Sample code	Graphene (wt%)	1st heating run			2nd cooling run		2nd heating run		
		T_{m1} (°C)	ΔH_{m1} (J/g)	X_{m1} (%)	T_c (°C)	ΔH_c (J/g)	T_{m2} (°C)	ΔH_{m2} (°C)	X_{m2} (J/g)
Neat PVDF	0.0	160.4	36.5	34.8	126.5	38.8	158.7	42.7	40.7
Graphene/PVDF_0.1	0.1	160.0	37.7	35.9	131.5	36.7	158.3	42.9	40.9
Graphene/PVDF_0.3	0.3	159.0	37.4	35.7	131.8	36.8	158.0	40.4	38.6
Graphene/PVDF_0.5	0.5	159.3	35.1	33.6	133.2	36.7	158.7	42.2	40.4
Graphene/PVDF_0.7	0.7	160.0	36.1	34.6	132.9	34.6	159.7	42.1	40.4
Graphene/PVDF_1.0	1.0	159.7	36.1	34.7	134.6	33.9	159.7	39.5	38.0
Graphene/PVDF_3.0	2.0	159.0	35.6	34.6	135.2	34.4	159.0	38.2	37.1
Graphene/PVDF_5.0	5.0	156.6	41.1	41.2	135.6	37.5	159.0	42.7	42.8
Graphene/PVDF_7.0	7.0	158.3	33.0	33.8	135.5	32.5	158.7	36.4	37.3
Graphene/PVDF_10.0	10.0	157.0	32.2	34.1	134.6	31.7	157.6	35.7	37.8

endothermic peaks remained unchanged, regardless of the graphene content in the nanocomposite films. From the DSC heating and cooling thermograms, melting and crystallization peak temperatures (T_m and T_c) and enthalpies (ΔH_m and ΔH_c) were evaluated and summarized in Table 1. The apparent crystallinity (X_m) of the nanocomposites could be calculated by considering the difference in graphene content of the nanocomposite films as follows:

$$X_m(\%) = \frac{\Delta H_m / \phi}{\Delta H_m^*} \times 100 \quad (1)$$

where ΔH_m^* is the melting enthalpy (104.5 J/g) [20] of the 100 % crystalline PVDF and ϕ is the weight fraction of PVDF in the nanocomposites. It was found that the apparent crystallinity (X_m) was almost identical for all the nanocomposite films, within the experimental error (Table 1). Therefore, it is reasonable to contend that, although the overall apparent crystallinity of the nanocomposites remains constant, graphene sheets dispersed in the nanocomposite films accelerate the formation of α-phase crystals as well as the overall melt-crystallization rate of PVDF.

Thermal Stability

Figure 5 presents TGA curves of graphene/PVDF nanocomposite films examined under the oxygen gas condition. For comparison, typical thermo-oxidative degradation temperatures ($T_{5\%}$ and $T_{50\%}$) for 5 % and 50 % weight loss for all the nanocomposite films were evaluated from the TGA curves and summarized in Table 2. It was found that $T_{5\%}$ and $T_{50\%}$ of the nanocomposite films increased with increasing the graphene content up to 1.0 wt% and then they decreased for the films with higher graphene contents above 3.0 wt%. For instance, $T_{5\%}$ and $T_{50\%}$ for the graphene/PVDF_1.0 film were measured to be 423 and 450 °C, which were 52 and 20 °C higher than those of the neat PVDF, respectively. The noticeable enhancement in thermal stability of the nanocomposite films

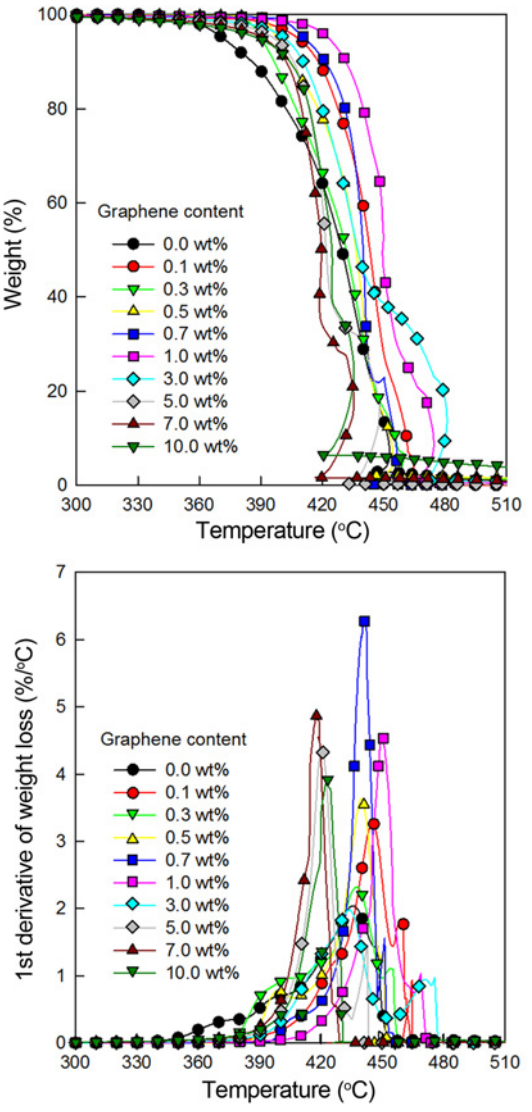

Figure 5. TGA thermograms of graphene/PVDF nanocomposite films with different graphene contents under the oxygen gas atmosphere.

Table 2. Thermo-oxidative degradation temperatures for 5 % and 50% weight loss ($T_{5\%}$ and $T_{50\%}$) of the neat PVDF and graphene/PVDF nanocomposite films under oxygen gas condition

Sample code	Graphene (wt%)	$T_{5\%}$ (°C)	$T_{50\%}$ (°C)
Neat PVDF	0.0	371.4	429.5
Graphene/PVDF_0.1	0.1	408.2	443.3
Graphene/PVDF _0.3	0.3	390.2	431.8
Graphene/PVDF _0.5	0.5	397.7	436.6
Graphene/PVDF _0.7	0.7	411.4	440.0
Graphene/PVDF _1.0	1.0	423.0	449.5
Graphene/PVDF _3.0	3.0	401.6	437.4
Graphene/PVDF _5.0	5.0	396.4	421.9
Graphene/PVDF _7.0	7.0	391.1	419.6
Graphene/PVDF _10.0	10.0	388.6	424.7

is believed to be caused by the barrier effect of 2-dimensional graphene sheets dispersed in the PVDF matrix to oxygen gas molecules.

Electrical Properties

Figure 6 displays electrical volume and surface resistivity of the graphene/PVDF nanocomposite films as a function of the graphene content. The electrical properties of the nanocomposite films changed noticeably from an insulator to nearly a semiconductor with the increment of graphene content. The electrical volume resistivity of the neat PVDF film was measured to be in the order of ~10^{14} Ω·cm. The electrical volume resistivity of ~10^{14} Ω·cm remained almost unchanged for the nanocomposite films with lower graphene contents of 0.1~1.0 wt% and then it decreased substantially to ~10^{6} Ω·cm for the films with higher graphene contents of 3.0~10.0 wt%. This dramatic decrement in the electrical resistivity of the graphene/PVDF films can be satisfactorily explained by the percolation theory, i.e., the electrical conduction path of interconnected graphene sheets in the nanocomposite films is formed at a critical graphene content between 1.0 and 3.0 wt%. It is also worthy to note that the electrical resistivity of ~10^{6} Ω·cm for the graphene/PVDF nanocomposites is low enough to show the performance of electrostatic dissipation and/or partial electromagnetic dissipation.

Mechanical Properties

To investigate the influence of graphene content on the mechanical properties of graphene/PVDF nanocomposites, dynamic storage modulus was measured as a function of temperature, as shown in Figure 7. For all the nanocomposite

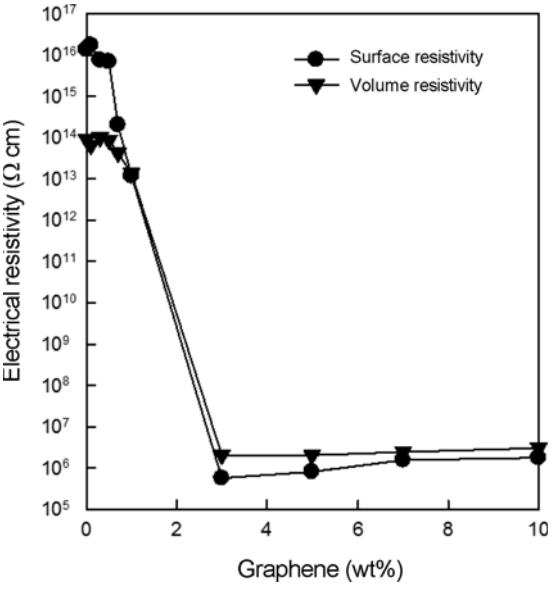

Figure 6. Electrical volume and surface resistivity of graphene/PVDF nanocomposite films as a function of the graphene content.

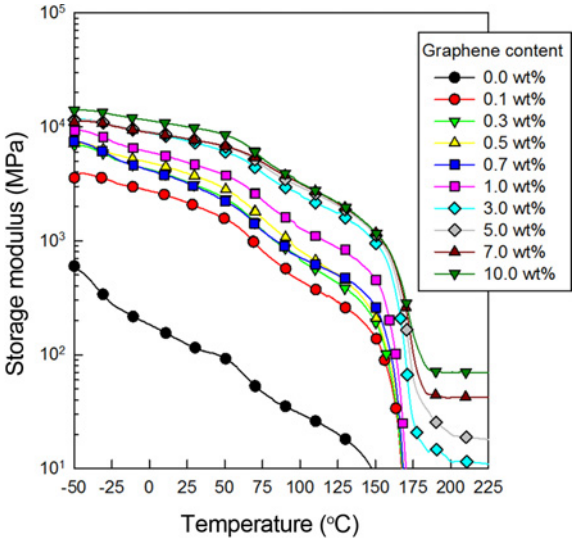

Figure 7. Temperature-dependent storage modulus of graphene/PVDF nanocomposite films with different graphene contents.

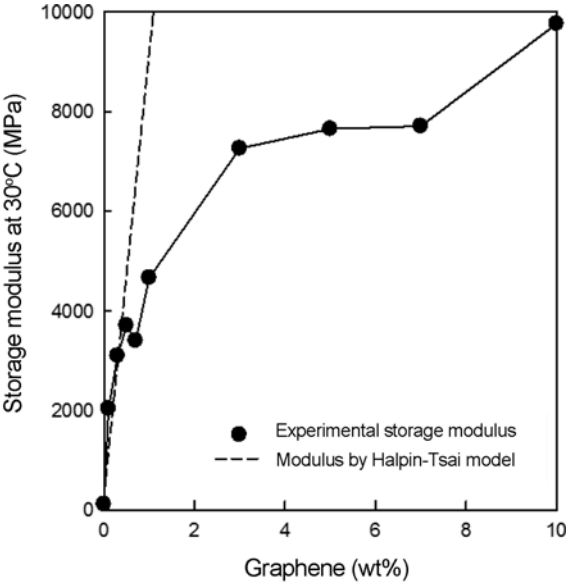

Figure 8. Experimental storage moduli of graphene/PVDF nanocomposite films at 30 °C as a function of the graphene content. The dotted line denote the theoretical modulus calculated by the Halpin-Tsai model.

films, the dynamic storage moduli decreased slightly With increasing the temperature from −50 to 150 °C, and they decreased rapidly above 150 °C due to the melting of PVDF crystals. When the dynamic storage moduli at room temperature for graphene/PVDF nanocomposite were compared, they were significantly increased with the graphene content up to 3.0 wt%. It indicates that the graphene platelets dispersed in the nanocomposites act as mechanical reinforcing fillers for the PVDF matrix.

For a deeper understanding the influences of graphene sheets on mechanical performance of the nanocomposite films, the storage modulus at 30 °C was plotted as a function of the graphene content, as can be seen in Figure 8, and it was compared with the results predicted by the Halpin-Tsai model. By assuming the random orientation of graphene sheets in the PVDF matrix, the theoretical composite modulus, $E_{composite}$, based on the Halpin-Tsai model is expressed as [21,22]

$$E_{composite} = \left[\frac{3}{8}\left(\frac{1+\frac{2}{3}\left(\frac{d_{graphene}}{t_{graphene}}\right)\eta_L V_{graphene}}{1-\eta_L V_{graphene}}\right)+\frac{5}{8}\left(\frac{1+2\eta_T V_{graphene}}{1-\eta_T V_{graphene}}\right)\right]E_{PVDF} \quad (1)$$

$$\eta_L = \frac{\frac{E_{graphene}}{E_{PVDF}}-1}{\frac{E_{graphene}}{E_{PVDF}}+\frac{2}{3}\left(\frac{d_{graphene}}{t_{graphene}}\right)}, \quad \eta_T = \frac{\frac{E_{graphene}}{E_{PVDF}}-1}{\frac{E_{graphene}}{E_{PVDF}}+2}$$

$$V_{graphene} = \left[1+\left(\frac{\rho_{graphene}}{\rho_{PVDF}}\right)\left(\frac{1-m_{graphene}}{m_{graphene}}\right)\right]^{-1}$$

where $E_{graphene}$ and E_{PVDF} are the modulus of graphene monolayer (1060 GPa) [9] and the experimental storage modulus (151 MPa) of the neat PVDF at 30 °C, respectively. $t_{graphene}$ and $d_{graphene}$ are thickness (~0.336 nm) and diameter (~10 μm) of graphene sheets prepared for this study. $V_{graphene}$, the volume fraction of graphene in the nanocomposites, which can be converted from the weight fraction of graphene ($m_{graphene}$), by adopting the graphite density ($\rho_{graphene}$=1.9 g/cm^3) and the density (ρ_{PVDF}=1.78 g/cm^3) of PVDF. As a result, the theoretical modulus by the Halpin-Tsai equation was calculated and presented as a dotted line in Figure 8. The experimental storage moduli at 30 °C were found to be quite consistent with the theoretical values for the nanocomposites with low graphene contents below 0.5 wt%, but they were far lower than the moduli for the nanocomposites with high graphene contents above 1.0 wt%. On the other hand, it should be mentioned that the Halpin-Tsai model is derived based on the assumptions such as the perfect interfacial adhesion between reinforcing graphene sheets and PVDF matrix, the perfect 2-dimensional planar structure of graphene sheets, and uniform dispersion of graphene sheets in the PVDF matrix. It is thus supposed that the huge difference between experimental and theoretical moduli of the nanocomposites with high graphene contents above 1.0 wt% is related with the presence of partial aggregates and wrinkling/crimping of graphene sheets in the PVDF matrix.

Conclusion

A series of graphene/PVDF nanocomposite films were

prepared by ultrasonication-assisted solution mixing and melt-compression. SEM images and X-ray diffraction patterns confirmed that the graphene sheets remained in the disordered state and they were well dispersed in the PVDF matrix. X-ray diffraction patterns of the nanocomposite films showed that the α-form crystals of PVDF were preferentially developed in the nanocomposite films during the melt-compression process. In DSC curves, the melt-crystallization temperatures of graphene/PVDF nanocomposite films increased with the increment of graphene content, which demonstrating that graphene nanoplatelets acted as effective nucleating agents for PVDF crystals. Thermo-stability of graphene/PVDF nanocomposites was significantly improved even at a low amount of graphene of 1.0 wt%, in comparison of the neat PVDF. The electrical volume resistivity of the nanocomposite films was decreased from ~10^{14} to ~10^{6} Ω·cm with increment of graphene content. The electrical percolation threshold of the graphene/PVDF nanocomposites was found to form at a critical graphene content between 1.0 and 3.0 wt%. From DMA results, storage moduli of nanocomposite films below T_m were remarkably increased with the introduction of graphene sheets.

Acknowledgement

This paper was supported by Research Fund, Kumoh National Institute of Technology.

References

1. H. Kawai, *Jpn. J. Appl. Phys.*, **8**, 975 (1969).
2. A. J. Lovinger, *Science*, **220**, 1115 (1983).
3. R. A. Vaia and E. P. Giannelis Eds., "Polymer Nanocomposites", American Chemical Society, Washington, 2001.
4. E. T. Thostenson, C. Li, and T.-W. Chou, *Compos. Sci. Technol.*, **65**, 491 (2005).
5. J. H. Koo, "Polymer Nanocomposites: Processing, Characterization, and Applications", McGraw-Hill, New York, 2006.
6. A. K. Geim and K. S. Novoselov, *Nature Mater.*, **6**, 183 (2007).
7. A. A. Balandin, S. Ghosh, W. Z. Bao, I. Calizo, D. Teweldebrhan, F. Miao, and C. N. Lau, *Nano Lett.*, **8**, 902 (2008).
8. J. Campos-Delgado, Y. A. Kim, T. Hayashi, A. Morelos-Gomez, M. Hofmann, H. Muramatsu, M. Endo, H. Terrones, R. D. Shull, M. S. Dresselhaus, and M. Terrones, *Chem. Phys. Lett.*, **469**, 177 (2009).
9. C. Lee, X. Wei, J. W. Kysar, and J. Hone, *Science*, **321**, 385 (2008).
10. K. S. Novoselov, A. K. Geim, S. V. Morozov, D. Jiang, Y. Zhang, S. V. Dubonos, I. V. Grigorieva, and A. A. Firsov, *Science*, **306**, 666 (2004).
11. R. Sengupta, M. Bhattacharya, S. Bandyopadhyay, and A. K. Bhowmick, *Prog. Polym. Sci.*, **36**, 638 (2011).
12. S. Ansari and E. P. Giannelis, *J. Polym. Sci. Pol. Phys.*, **47**, 888 (2009).
13. V. Eswaraiah, K. Balasubramaniam, and S. Ramaprabhu, *J. Mater. Chem.*, **21**, 12626 (2011).
14. J. Cao, Y. Wang, Y. Luo, W. Yang, B.-H. Xie, and M.-B. Yang, *Polym. Int.*, **61**, 1031 (2011).
15. P. Han, J. Fan, L. Zhu, C. Min, X. Shen, and T. Pan, *J. Nanosci. Nanotechnol.*, **12**, 7290 (2012).
16. L. Staudenmaier, *Ber. Dtsch. Bot. Ges.*, **31**, 1481 (1898).
17. H. C. Schniepp, J.-L. Li, M. J. McAllister, H. Sai, M. Herrera-Alonso, D. H. Adamson, R. K. Prudhomme, R. Car, D. A. Saville, and I. A. Aksay, *J. Phys. Chem. B.*, **110**, 8535 (2006).
18. M. J. McAllister, J.-L. Li, D. H. Adamson, H. C. Schniepp, A. A. Abdala, J. Liu, M. Herrera-Alonso, D. L. Milius, R. Car, R. K. Prudhomme, and I. A. Aksay, *Chem. Mater.*, **19**, 4396 (2007).
19. J.-E. An, G. W. Jeong, and Y. G. Jeong, *Fiber. Polym.*, **13**, 507 (2012).
20. S. Schneiger, X. Drujon, J. C. Wittman, and B. Lotz, *Polymer*, **42**, 8799 (2001).
21. J. C. Halpin and S. W. Tsai, "Effects of Environmental Factors on Composite Materials", US Air Force Materials Laboratory, Dayton, Ohio, 1969.
22. J. C. Halpin and J. L. Kardos, *Polym. Eng. Sci.*, **16**, 344 (1976).